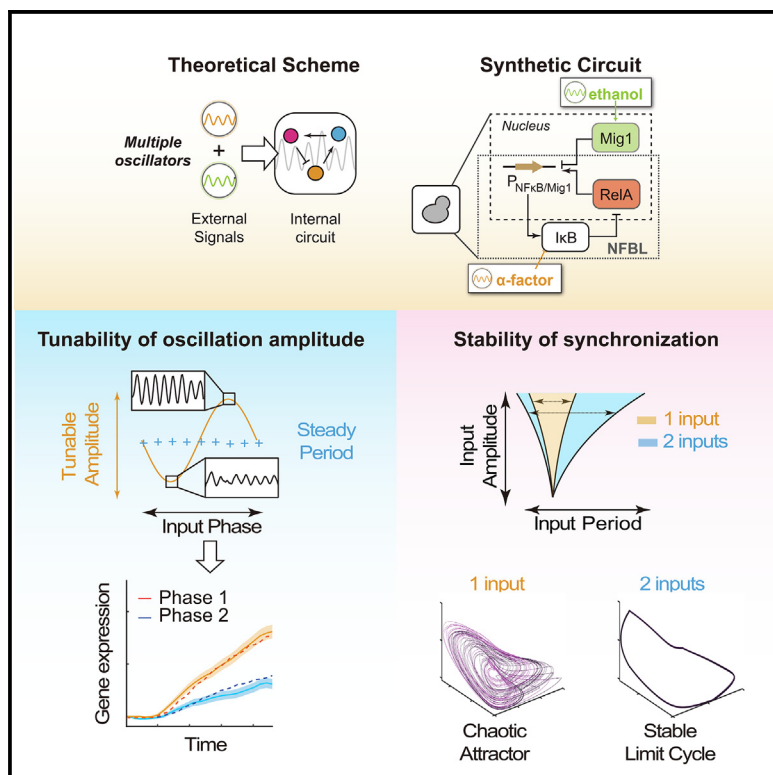


Coupled oscillator cooperativity as a control mechanism in chronobiology

Graphical abstract



Authors

Mathias S. Heltberg, Yuanxu Jiang,
Yingying Fan, ..., Qi Ouyang,
Mogens H. Jensen, Ping Wei

Correspondence

mjhjensen@nbi.dk (M.H.J.),
ping.wei@siat.ac.cn (P.W.)

In brief

Heltberg et al. reveal the cooperative regulatory mechanism between the intrinsic and two extrinsic oscillators with synthetic biology approach, which enables stabilized entrainment and decoupled amplitude modulation through variation in phase difference. This generalizes the theory of coupled oscillators and provides insights for dynamic control in living cells.

Highlights

- A synthetic oscillatory circuit responding to periodic α -factor and ethanol is designed
- Two oscillatory signals stabilize the entrainment
- Phase modulation between oscillatory signals controls the amplitude
- Oscillation amplitude directly affects downstream gene expression levels



Article

Coupled oscillator cooperativity as a control mechanism in chronobiology

Mathias S. Heltberg,^{1,2,5} Yuanxu Jiang,^{1,3,5} Yingying Fan,^{1,3,5} Zhibo Zhang,³ Malthe S. Nordentoft,² Wei Lin,³ Long Qian,³ Qi Ouyang,³ Mogens H. Jensen,^{2,*} and Ping Wei^{1,3,4,6,*}

¹Center for Cell and Gene Circuit Design, CAS Key Laboratory of Quantitative Engineering Biology, Shenzhen Institute of Synthetic Biology, Shenzhen Institute of Advanced Technology, Chinese Academy of Sciences, Shenzhen 518055, China

²Niels Bohr Institute, University of Copenhagen, 2100 Copenhagen, Denmark

³Center for Quantitative Biology, Academy for Advanced Interdisciplinary Studies, Peking University, Beijing 100871, China

⁴Faculty of Synthetic Biology, Shenzhen Institute of Advanced Technology, Chinese Academy of Sciences, Shenzhen 518055, China

⁵These authors contributed equally

⁶Lead contact

*Correspondence: mhjensen@nbi.dk (M.H.J.), ping.wei@siat.ac.cn (P.W.)

<https://doi.org/10.1016/j.cels.2023.04.001>

SUMMARY

Control of dynamical processes is vital for maintaining correct cell regulation and cell-fate decisions. Numerous regulatory networks show oscillatory behavior; however, our knowledge of how one oscillator behaves when stimulated by two or more external oscillatory signals is still missing. We explore this problem by constructing a synthetic oscillatory system in yeast and stimulate it with two external oscillatory signals. Letting model verification and prediction operate in a tight interplay with experimental observations, we find that stimulation with two external signals expands the plateau of entrainment and reduces the fluctuations of oscillations. Furthermore, by adjusting the phase differences of external signals, one can control the amplitude of oscillations, which is understood through the signal delay of the unperturbed oscillatory network. With this we reveal a direct amplitude dependency of downstream gene transcription. Taken together, these results suggest a new path to control oscillatory systems by coupled oscillator cooperativity.

INTRODUCTION

Biological oscillations ubiquitously control fundamental biological processes, such as the circadian clock,^{1–4} development,^{5,6} neuronal signal processing,^{7,8} and transcription factor (TF) responses.^{9–14} In particular, the oscillations in TFs such as p53 and nuclear factor κB (NF-κB) seem to be an integral part of cellular regulation, but the function and stabilization of these signals are still far from understood^{15,16} even though recent work has suggested mechanistic effects of p53 oscillations.¹⁷

When one oscillator is affected by a second, the resulting dynamics of the first is understood through the theory of Arnold tongues.¹⁸ These tongues predict how small oscillations will lead to entrainment, where two oscillators synchronize, whereas larger oscillations will lead to complex dynamics such as period doublings, multistability, and chaotic behavior.¹⁹ This can in turn affect a cascade of downstream proteins, and therefore it is fundamental for the cellular networks to be able to control the bifurcations into complex dynamics.²⁰ Biological oscillators appear frequently on the cellular scale, and the coexistence of multiple oscillators has been revealed in different biological systems.^{21–26} Therefore, our main questions in this work are the following. How will the combination of oscillatory signals affect the controllability of an oscillatory system? In particular, will

this stabilize synchronization and robustness or conversely lead to complex dynamics? Furthermore, how can the dynamic aspects of TF concentration affect downstream gene stimulation and thereby the state of the cell?

To shed light on this problem, we constructed a synthetic oscillator in yeast cells (*S. cerevisiae*) and connected it with two natural signaling pathways that sense the α-mating pheromone (α-factor) and ethanol, respectively. We also derived a simple mathematical model to predict the behavior of the system under two oscillatory signals. Fundamentally, our aim was to understand whether the addition of two external signals would lead to more complex dynamics or stabilize the oscillations and thus lead to a higher degree of order. From the point of view of the Arnold tongues, both outcomes would be plausible, and therefore it is important to understand the resulting effect. Here, our study reveals that a combination of two external signals leads to a larger entrainment regime and stabilizes the oscillations by reducing the standard deviations in the periods. Furthermore, with two external signals, the phase difference between these affects the amplitude of the TF, while keeping the frequency constant. We demonstrated through mathematical modeling that the amplitude reaches maximal when the difference in phases corresponds to the phase lag between proteins in the oscillatory but non-perturbed system. To further validate these findings, we



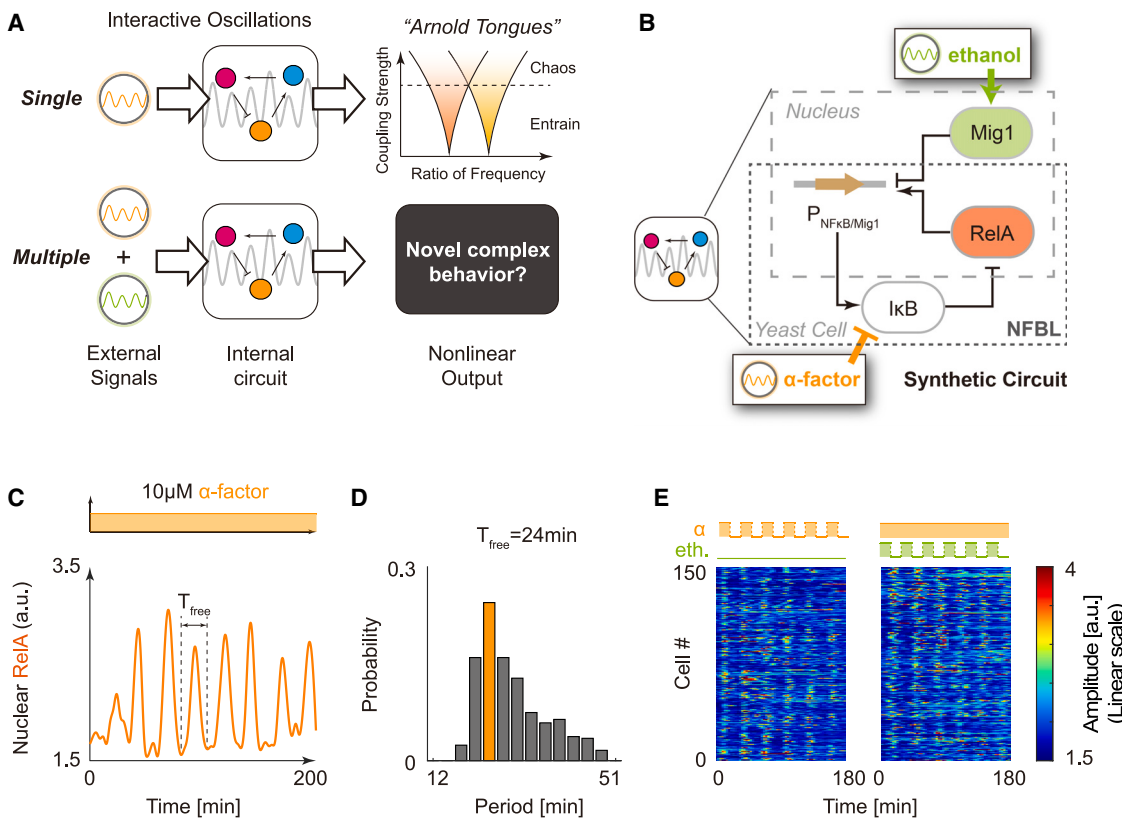


Figure 1. RelA dynamics and periodic stimulation

- (A) Schematic figure of coupled oscillators in biological systems. The output of a single coupling (upper panel) is described by the Arnold tongues. Coupling with multiple oscillators (lower) remains unexplored.
- (B) Schematic design of the synthetic oscillatory circuit in yeast. The α -factor and ethanol act as two oscillatory inputs.
- (C) Example of single-cell nuclear RelA level under continuous 10 μM α -factor.
- (D) Distribution of oscillatory period.
- (E) Nuclear RelA level of the cell population under oscillatory α -factor input (left) and oscillatory ethanol input with basal α -factor (right).

investigated three canonical mathematical models and find these results to be consistent. Finally, by applying the above results to stimulate the amplitude of oscillations and measuring the concentration of downstream proteins, we validated that enhanced amplitudes in TF dynamics also promote the downstream protein production. In total, these results suggest that living organisms can use multiple oscillatory inputs to optimize the dynamical signals and thereby obtain fine-tuned regulation.

RESULTS

Experimental setup allows stimulation of two external oscillatory signals

When one oscillatory system is affected by an external oscillatory signal, entrainment regions known as Arnold tongues will emerge. These define regimes, where one can perturb the external oscillatory signal, which directly causes the oscillatory system to follow, resulting in a higher degree of control and order of the oscillations. However, for large values of external stimulation, the coupling of an external oscillatory signal can lead to complex dynamics and chaos. Since an increasing number of oscillators have been revealed in cells, it is a fundamental and

unresolved question: what will happen when a second oscillator is added to the network? This is schematized in Figure 1A.

To investigate this, we constructed a synthetic oscillatory circuit utilizing the human NF- κ B system, which consists of the TF RelA and its inhibitor I κ B. RelA is generally sequestered by I κ B at resting state and is released to the nucleus upon the addition of α -factor, which induces the degradation of I κ B. The transcription of I κ B is promoted by nuclear RelA and repressed by nuclear Mig1; the latter is a natural stress-responsive transcription repressor in yeast and can be activated by ethanol. In short, both α -factor and ethanol in our system promoted the nuclear import of RelA but on either post-translational or transcriptional levels. With a microfluidic system, the α -factor and ethanol could be added in precisely defined oscillatory patterns (Figure S1). Therefore, our system represented a simple case of three interacting oscillators, with two independent oscillatory inputs affecting different parts of the internal synthetic oscillatory signaling system (Figure 1B; STAR Methods).

After constantly adding the fixed level of α -factor, the activation of RelA (nuclear import) exhibited oscillatory dynamics, and we quantified the free oscillation period to be 24 min (Figures 1C and 1D). Next, we stimulated the system periodically

by introducing a square wave, thus changing either the level of α -factor or ethanol alone for a period of 30 min. In doing so we observed clear entrainment to both external stimulations (Figure 1E). Thus, the synthetic system could be effectively coupled to two different external oscillatory signals, promoting our further exploration to test the responses from combined inputs. We first compared the experimental results to mathematical predictions, by deriving a simplified model based on a previously published model²⁷ and aligning it with current observation of oscillatory period and amplitude (Figure S2). In this process, we reduced the number of variables and free parameters, by applying the assumption that the total amount of RelA is constant and by assuming that the rate of mRNA to export the nucleus before translation was fast compared to the other rates. The parameters were chosen similarly to the previous model by Zhang et al. and further reduced by for instance assuming a Hill coefficient of 2 (representing the biophysical mechanism of RelA as a dimer) instead of the previous value of 3. Overall, this model reduces the number of parameters and simplifies the mathematical description.

Thereby, we had successfully constructed a biological system with one oscillator (RelA) that could be stimulated by two external oscillatory signal inputs (α -factor and ethanol). Next, we investigated how these two combined could affect the dynamics of RelA.

Stabilization of oscillations from two external oscillatory signals

Investigating non-monotonic pattern of controllability, we first tested how the two combined oscillatory signals would affect the synchronization regions of the Arnold tongues *in silico*. We constructed the Arnold tongue map for the addition of α -factor only (Figure 2A, left) and by inspecting the synchronization regions for fixed amplitude, known as “devil’s staircase,” we found an enlargement of the entrainment plateau for the combined input of α -factor and ethanol (Figure 2A, middle, blue curve). Note that the Arnold tongue diagram (Figure 2A, left) serves as a way to understand the structure of entrainment and is only visualized for the numerical studies of α -factor, since this represents the original external addition and ethanol is a secondary addition. To verify this theoretical finding, we tuned the input oscillation period from 10 min to 50 min and quantified the output oscillations (Figure S3). The results confirmed the larger plateau under the combined input conditions in comparison to single input conditions (Figure 2A, right). We expected that the resulting plateau would be dominated by one of the plateaus of the single external signal and possibly have the width of the mean of the two individual stimulations. However, we noted that this result was not a linear combination of the two inputs individually but rather a general broadening of the Arnold tongues in a cooperative effect even though the two inputs were completely independent.

Next, we investigated how oscillations are stabilized in the regime of entrainment evaluating the oscillatory robustness. For simulations we applied the Gillespie algorithm²⁸ and calculated the power spectrum of the simulated traces. We observed that the fraction of identified entrained cells increased dramatically for the addition of two inputs (Figure 2B). Here, we had chosen the signals so they individually entrained the oscillator

approximately to the same extent, and thereby we could estimate the effect of two external oscillatory signals. We stress that this does not mean that external α -factor and ethanol will entrain with equal coupling strength, but it does reveal that the oscillators in combination affect the system better than they do individually. This was confirmed in the experimental traces by calculating the entrainment index of cells in the three conditions (Figure 2C). Note that in these results we have kept the phase difference between the two external oscillators fixed at $3\pi/2$. To follow up on this, we estimated the standard deviation of all identified periods as a measure of the oscillatory signal strength and found this reduced for double stimuli (Figure 2D, left), which was confirmed in the model (Figure 2D, right). Finally, we calculated the autocorrelation of the oscillatory signal, by aligning all cells and calculating the average value as a function of the time added. For non-entrained cells this drops quickly to 0, whereas oscillations will persist for entrained signals with largest amplitude for the strongest entrained samples. The experimental and mathematical findings agreed well (Figure 2E), confirming that the combined addition of oscillatory inputs increased the entrainment strength of the system.

The transition into chaotic dynamics for large external amplitudes is fundamental for Arnold tongues.¹⁹ Since we have found a broadening entrainment plateaus, an obvious question is whether the double oscillatory inputs would trigger a transition into chaotic dynamics? To explore this, we amplified the signal of the single external input (α -factor) and found regions of chaotic dynamics, defined by a positive Lyapunov exponent, where traces separated infinitesimally from each other diverge in time²⁹ (Figure 2F). We then tested this with the double input and found a regular, oscillatory dynamics indicated by a stable limit cycle (Figure 2G). To be convinced by this observation, we varied the amplitude of α -factor, keeping the ethanol fixed at different levels, and found that the transition into chaotic dynamics could be delayed by the addition of a second oscillatory input (Figure 2H). Based on these observations, we concluded that two independent, external signals possessed the ability to increase the controllability of the internal oscillation by increasing the entrainment properties, stabilizing the periods and delaying the onset of chaos.

Phase-dependent amplitudes allow fine-tuned regulation

We next aimed to test how two external inputs could be used to tune the internal system. Since two inputs may combine in different orders, it would be natural to ask whether the different combinatorial patterns of inputs can tune the oscillatory dynamics. We combined the two oscillatory inputs with fixed periods and variable phases, which is described by a phase difference, p , ranging from 0 to 2π (Figure 3A). Here we observed that the experimental traces showed different output dynamics among these conditions (Figure 3B). This is visualized by calculating the average in each frame, revealing a larger amplitude for the phase difference at $3\pi/2$ compared to $\pi/2$, which is further confirmed by performing a time-embedding algorithm on the time series (Figure 3C).

We extracted and quantified the oscillation amplitude for all well-behaved cells and revealed an interesting non-monotonic pattern, which leads to maximal amplitude at $p = 3\pi/2$ (Figure 3D,

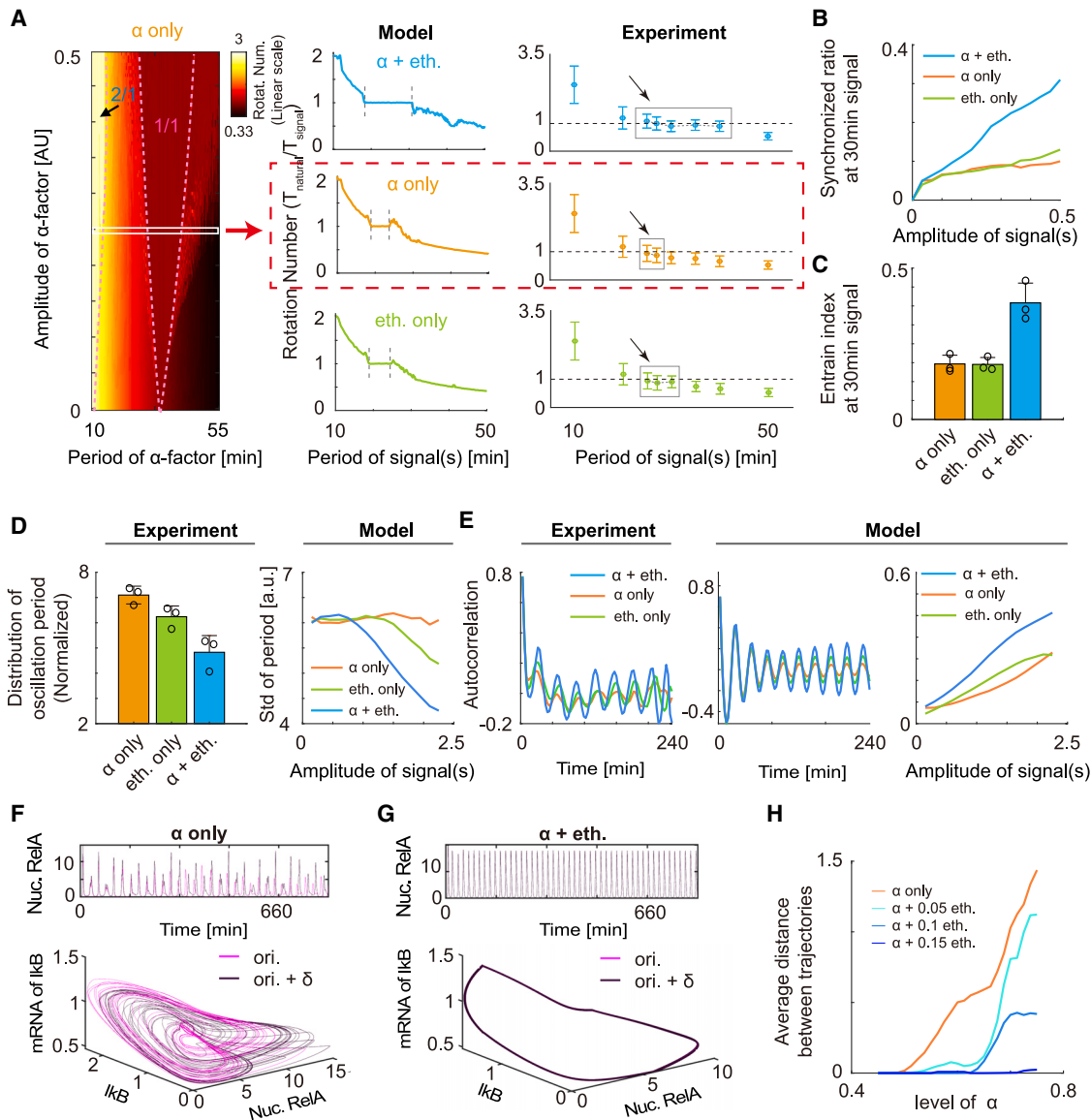


Figure 2. Oscillatory robustness with double stimuli

- (A) Simulation of Arnold tongues, applying external oscillation in α -factor (left). Rotation number as function of external frequency, with single and double stimuli (middle). Experimental results for all conditions (right), bars represent SEM of single cells.. The phase difference between α -factor and ethanol is $3\pi/2$ in all double input conditions.
- (B) Ratio of synchronized cells for external period at 30 min (Simulation).
- (C) Entrain index (EI) calculated for single and double stimuli (Experiments). Bars represent the standard deviation of three technical replicates.
- (D) Standard deviation on periods in experiments (left, bars represent the SD of three technical replicates) and in simulations (right) as a function of external amplitude (right).
- (E) Average autocorrelation as function of time delay in experiments (left) and simulations (middle) shown as function of external amplitude (right).
- (F) Simulated time trace (above) and the related phase space (below) for stimulation with only α -factor.
- (G) Same as (F) but for stimulation with α -factor and ethanol.
- (H) Average distance between two curves initially separated by 0.01% as a function of the external amplitude.

gray curve). This was consistently reproduced by the mathematical model, and therefore we concluded that varying the phase difference of the input oscillations could be a way to achieve the fine-tune of oscillatory signaling dynamics (Figure 3D, cyan curve). The result can intuitively be understood as follows: when ethanol is added after α -factor, it represses the feedback

induction of $\text{I}\kappa\text{B}$, causing insufficient re-sequestration of RelA and correspondingly insufficient nuclear import of RelA during the next period. Conversely, if ethanol is added ahead of α -factor, the two signals may work in coordination to decrease the level of $\text{I}\kappa\text{B}$, since the timescale of transcriptional regulation is typically longer than post-translational regulation, in turn causing

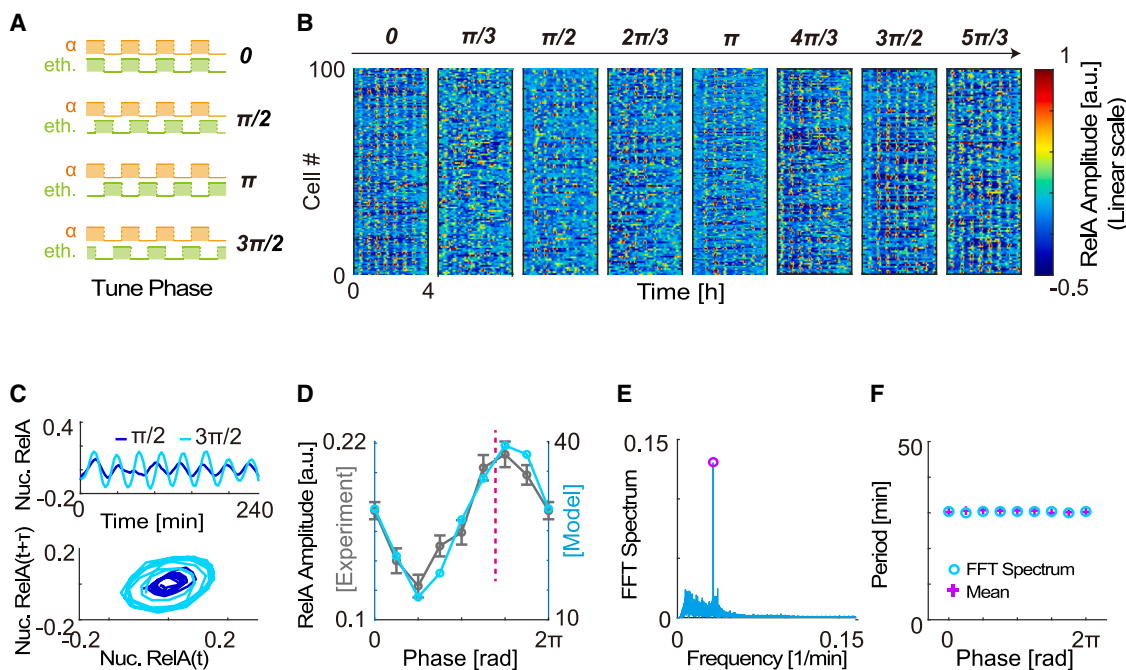


Figure 3. Tunability of RelA dynamics through phase variation

- Schematic figure of experimental design.
- Visualization of intensity for experimental cells with 8 phase differences. α -factor ahead of ethanol is designated as positive.
- Average time trajectory for cells with phase differences $\pi/2$ and $3\pi/2$ (above). Phase space of the same data, visualized by applying time embedding (below). We used 3 datapoints in the embedding process, which correspond to a time 3*(time between two data points).
- Variation of the oscillation amplitude as a function of phase difference for experiment (gray) and model (cyan). Bars represent the SEM.
- FFT spectrum for all traces with phase difference 2π .
- Average period for all traces calculated by FFT (circles) and peak finding (crosses).

an increase in oscillation amplitude. In the mathematical model, we could measure the phase difference between the RelA and mRNA for I κ B when the system is not perturbed by external oscillatory signals. We hypothesized that the optimal phase difference between the external oscillatory signals should match the normal phase difference in the entities they affected, and here we found a good agreement (Magenta line Figure 3D). This leads to a major insight in the systems of two external oscillatory signals. Since a limit cycle has at least two dimensions, there will be a natural phase difference between the variables, and in order to gain the optimal amplitude response, these should match each other. This is further investigated in the following section. Inspired by this, we also tried to let all parameters be affected by a minor oscillation, and here we found that a random distribution of phase differences clearly enhances the oscillation amplitude compared to the situation where all are in the same phase (Figure S4).

To ensure that our observation was not due to a variation in the period, we calculated the fast Fourier transform (FFT) spectrum for all traces (Figure 3E) and obtained the frequency with highest power spectrum. Furthermore, we also calculated the periods based on each peak, and by grouping these, we found a strong correspondence for all input phase differences that showed entrainment and equal periods (Figure 3F). Thus, one can alter the amplitude without affecting the frequency by tuning the phase difference between two input oscillators,

something that is typically difficult for oscillatory signals in biology.

Generalization to other models suggests universal behavior

At this stage our work has revealed that two external oscillatory signals could improve the entrainment and that varying their phases would affect the amplitude of the internal oscillator. It was thus crucial to test whether these observations could be applied to a broader spectrum of oscillations, and therefore we turned to mathematical modeling.

We decided to test these results on three different models (note that all parameters can be found in Table S2).

Van der Pol oscillator³⁰
p53 oscillator³¹
NF- κ B oscillator¹¹

We started out with the Van der Pol model, which is based on a physical setup from electrical engineering (Figure 4A) but is described mathematically similar to a harmonic oscillator, with the addition of two nonlinear terms. For this model we used additive stimulation, so that each of the two variables (x and y) had an addition of an oscillation. Since x is “produced” by y , and y is for small values of μ “degraded” by x , we subtracted the oscillation in x , in order to mimic the addition of oscillators of the

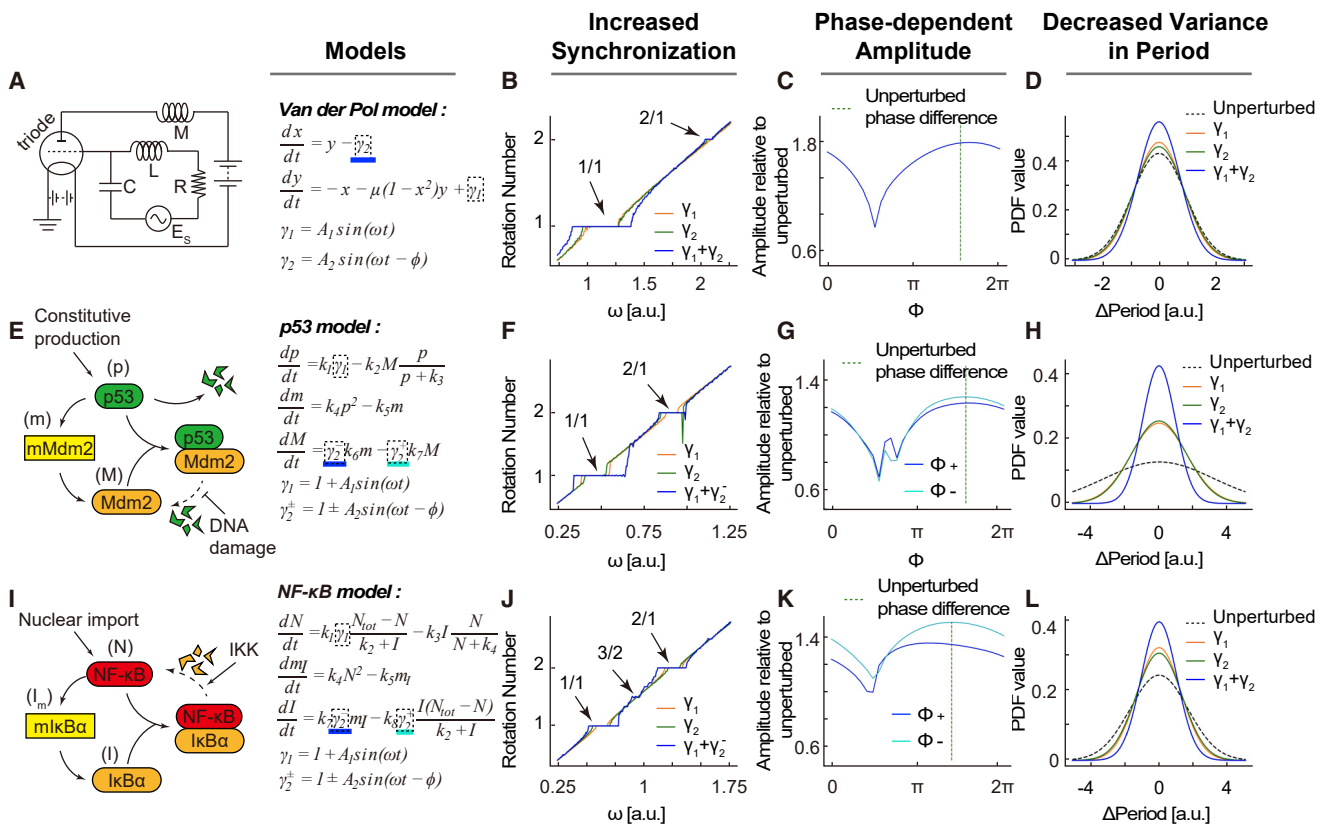


Figure 4. Coupled oscillator cooperativity revealed in generalized biological and nonbiological systems

- (A) Schematic version of the electrically inspired Van der Pol network and the resulting equations.
- (B) Devil's staircase when varying ω . Here ϕ is $3\pi/2$ as in the experimental setting.
- (C) Amplitude of variable y when shifting the phase difference. Here ω is constant at 1.
- (D) Standard deviations in the periods of y , measured for the unperturbed system, the addition of γ_1 and γ_2 individually and combined. Here ω is constant at 1 and ϕ is $3\pi/2$.
- (E) Schematic version of the p53 network and the resulting equations.
- (F) Same as (B) but for the p53 network.
- (G) Same as (C) but for the p53 network with ω constant at 0.5.
- (H) Same as (D) but for the p53 network with ω constant at 0.5 and ϕ is $3\pi/2$.
- (I) Schematic version of the simple NF-κB network and the resulting equations.
- (J) Same as (B) but for the NF-κB network.
- (K) Same as (C) but for the NF-κB network with ω constant at 0.6.
- (L) Same as (D) but for the NF-κB network with ω constant at 0.6 and ϕ is $3\pi/2$.

experimental setup. Here we found that the width of the devil's staircase did increase for the addition of two external oscillatory signals in contrast to each of these individually (Figure 4B). Next, we varied the phase difference, and again we found that the amplitude did show a phase dependence and that the optimum was predicted by the phase difference in the non-perturbed system (Figure 4C). Finally, we added stochasticity to the system, and since x and y are continuous variables that will become negative in this system, we applied Langevin noise. This also tested the robustness to different variants of added stochasticity. Here we found that the addition of both oscillators individually stabilized the system, but in combination they could reduce the variance of the periods even further (Figure 4D).

We then turned to a more biologically inspired system, namely the p53 network. This is an archetypical negative feedback loop

(Figure 4E), and we therefore expected that we would observe some of the main features for two external oscillatory signals. The oscillations were introduced as a parameter perturbation, and we hypothesized that one external oscillatory signal should indeed depend on whether it stimulated or inhibited the variable to which it was added. In particular, this should result in a phase response shifted exactly by π , and we incorporated this effect by having a negative sine term on the positive part of the differential equation for M (since this is a response of p53) and a positive sine function on the negative part of the differential equation. These were termed $\gamma^{-/-}$ respectively. First, we found that the entrainment plateaus of the devil's staircase indeed increased, both the 1/1 and the 2/1 plateau (Figure 4F). Next, we investigated the effect on the amplitude of p53, and here we found similar behavior, and in particular we confirmed our hypothesis that

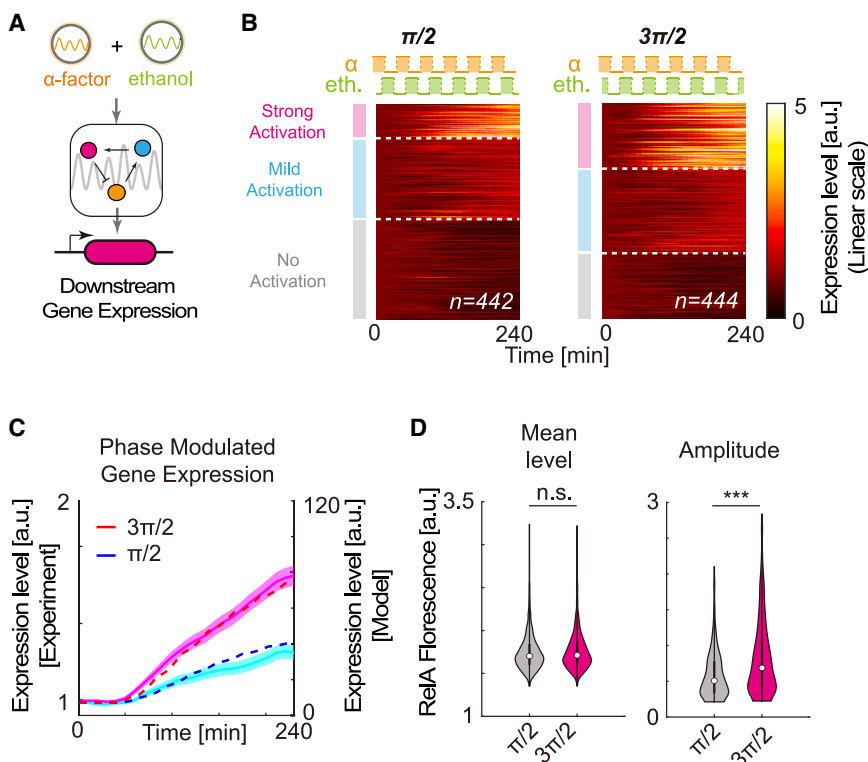


Figure 5. Downstream stimulation following perturbed RelA dynamics

(A) Schematic figure showing upstream stimulation and the effect on downstream genes.

(B) Intensity for gene expression for strong ($MFI > 2$), mild ($1 < MFI < 2$), and no activation ($MFI < 1$). MFI , mean fluorescence intensity. Phase difference is $\pi/2$ (left) and $3\pi/2$ (right), with α -factor ahead of ethanol designated as positive.

(C) Concentration of downstream proteins from stimulation with $\pi/2$ (cyan) and $3\pi/2$ (magenta). Data shown for simulations (dotted lines) and experiments (full lines). Shaded regions represent SEM.

(D) Distribution of oscillatory RelA behavior with $\pi/2$ (gray) and $3\pi/2$ (magenta) for the mean level (left) and amplitudes (right). A Wilcoxon rank-sum test was used to quantify the significance and a p value < 0.001 “***” was designated as statistically significant.

more expression in the case of $\rho = 3\pi/2$, agreeing well with model predictions (Figure 5C). Here we used the downstream expression model previously used by Heltberg et al.^{20,34} We computed the mean level of RelA and found no significant difference between the two condi-

tions (Figure 5D). This confirmed that the enhancement of protein production was purely caused by the variation in amplitude. Previous setups have not been able to change the amplitude while keeping the mean level and frequency constant, but with this setup of two external oscillatory signals, we can confirm this hypothesis. We also systematically explored which parameters could result in enhancement of the downstream protein production when stimulated in combination with α -factor (Figure S4) and found that the output expression level experienced a crossover effect when enhancing the external oscillations.

In total, our results demonstrate that oscillatory inputs together can provide enhanced controllability on chronobiological systems. This controllability is reflected in both the stability level of single-cell oscillations and synchronization and the tunability of oscillatory dynamics (Figure 6). These observations can be generalized to guide the understanding of biological systems and may explain how cells can navigate in the presence of multiple oscillatory signals that could be included by circadian rhythms, cell cycle, or even downstream effects of TF oscillations on the timescale of hours. This work provides a plausible explanation on how such signals can increase the regularity of periodic signals.

DISCUSSION

In this work we have revealed how two external oscillatory signals can be used as a way to stabilize the oscillations of an internal oscillator. Furthermore, we have revealed that the phase difference between the two external oscillatory signals can be a very important parameter, since it allows us to shift the amplitude of the internal oscillator and therefore could be a control

the effect of external oscillatory signals could be predicted by their role in the negative feedback loop (Figure 4G). Finally, we tested the variance of the periods, by simulating the stochastic version of the system using Gillespie algorithm and did again confirm that two external oscillatory signals could stabilize the oscillations (Figure 4H). Finally, we repeated this for network of NF- κ B inspired by the simple mathematical model (Figure 4I). Here we again confirmed all the above observations (Figure 4J–4L).

Taken together, this mathematical investigation suggests general features for an oscillatory system that is perturbed by two external oscillatory signals. Next, we wanted to investigate whether the resulting dynamics of a TF could also stimulate the downstream protein production.

Oscillation amplitudes determine downstream protein production

Since oscillations in TFs have been accepted to be an integral part of cell regulation,^{10,12} we investigated how the coupled oscillatory stimulation of the TF could affect the downstream protein production. Previous work has identified several roles for oscillations in regulating gene transcription,^{32,33} but since amplitude and frequency of TF oscillations are typically correlated, the actual role of amplitudes has not been completely understood.

Since our results showed amplitude variations for fixed frequency, we investigated this by introducing an mCherry fluorescence reporter into the system (Figure 5A). We identified that signals with phase difference $\rho = 3\pi/2$ induced a higher protein level compared to conditions with $\rho = \pi/2$ (Figure 5B). We measured the protein level as function of time and observed

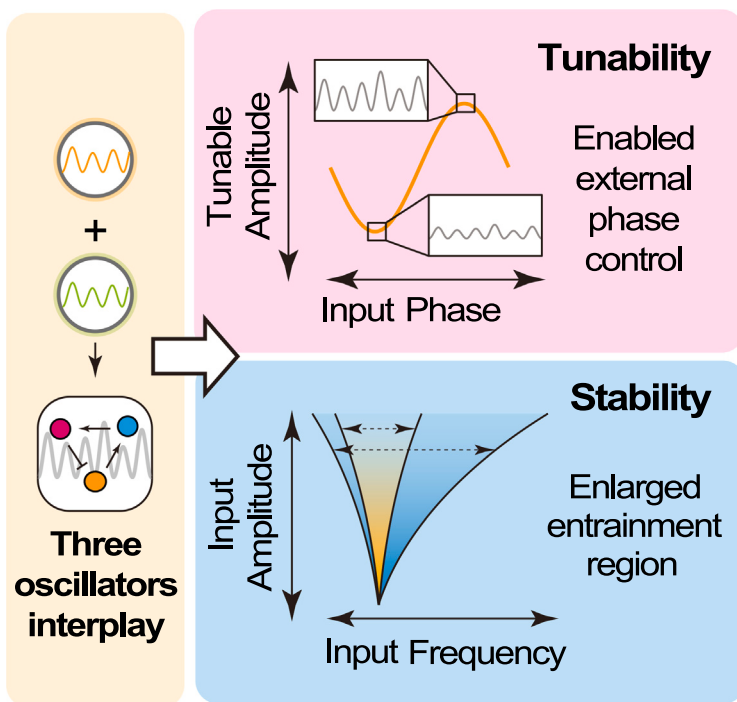


Figure 6. Working model outlining how three oscillations interplay and perform new dynamic behaviors

Upper: The amplitude-only modulation of the internal oscillator enabled by tuning the relative phase of two oscillatory signals.

Lower: The stability of the entrainment was enhanced by additional external oscillations.

mechanism in chronobiology. We finally applied this change of amplitude, to test how downstream proteins were affected by this, and found that an increasing amplitude can enhance the stimulation of downstream genes as predicted by the mathematical model.

We introduced a mathematical model that simplifies previous models of the RelA in the synthetic circuit. We applied the previously applied degradation terms of the protein complex involving a Michaelis-Menten term.^{27,35} Here it is important to note that this formulation delivers exact results when substrate concentrations are much larger than the concentrations of enzymes that catalyze the reactions. We believe that this is the relevant parameter range for the synthetic biological system we are investigating, but using these terms in differential equations outside of its domain of validity can affect the resulting dynamics and thereby reduce the reliability of the model.³⁶ Therefore, it would be of interest in future work to further test the model in different biological settings in order to enhance the fundamental understanding of its limits.

The idea that multiple oscillators can interact is old and was originally pioneered by the work of Kuramoto,³⁷ and aspects of multiple interacting oscillators has typically been performed using versions of the Kuramoto model.^{38–40} In this work, we started out from the theory of Arnold tongues so that one internal oscillator depends on the external oscillatory signal but not the other way around, and thereby they do not mutually influence each other as happens in Kuramoto models. Furthermore, since the Kuramoto model only describes the dynamics of a phase, it does not model the amplitudes and potentially complex dynamics from the amplitudes that in a biological setting can be crucial.

We have in this work studied the effect of phase difference variation from two external oscillatory signals on the amplitude of an internal oscillator. We observed that for all models it resulted in an optimum, and while for the experimentally studied system we found that the change in amplitude was on average zero, our simple models, introduced as a generalization of the results, suggested that the change in amplitude could often have a greater mean level, thereby enhancing the amplitude for almost all values of external phases. Based on this, we believe there is an interesting aspect in studying how the entrainment plateau of the Arnold tongues might scale with the phase difference between the two external signals. To study this, it is important to emphasize that, for one external oscillatory signal, the locked phase to the internal oscillator varies across the Arnold tongue with exactly π .⁴¹ This means that

a change in the frequency of the external oscillatory signal affects the relative phase to the internal oscillator in the locked state, and this might affect the value of the optimal phase difference. Also, it is an open question how the two external oscillatory signals can enhance the entrainment plateau in the regimes where none of the two signals individually can lead to any entrainment. We believe that this is a very important question to investigate in depth.

The enhanced entrainment allows more robust synchronization and can be important in different biological settings. Our work reveals that a simple addition of an external oscillator can improve the synchronization and stabilize the system. Previously it has been reported that the robustness of circadian entrainment to daylight variability can be optimized by affecting the linear response properties of an oscillator to vanishingly small light input.^{42,43} Recent work has also revealed how clock-modulating pharmaceutical drugs can affect and stabilize the circadian rhythm,⁴⁴ for instance by inhibition of casein kinase 1⁴⁵ or affecting the level of photosensitivity.⁴⁶ Furthermore, it has also previously been studied that the effect of a positive feedback loop in the protein network might stabilize the entrainment region²⁴ as well as stochastic noise can enhance the entrainment level for a population of cells.⁴⁷ Thereby, it seems possible that life applies a fascinating toolbox of approaches to enhance the entrainment in different external settings.

Finally, with the method presented here it is possible to independently address the influence caused by oscillation amplitude on gene expression, thus providing accurate knowledge to the field of dynamic control. We term the phenomenon of controllability by many oscillatory signals as coupled oscillator cooperativity, since their independent contributions lead to a system with

a higher degree of controllability than each of their individual contributions. We believe that these results can guide and influence our understanding of oscillatory networks not only in the field of gene regulation but in physics, biology, and chemistry in general.

STAR★METHODS

Detailed methods are provided in the online version of this paper and include the following:

- **KEY RESOURCES TABLE**
- **RESOURCE AVAILABILITY**
 - Lead contact
 - Materials availability
 - Data and code availability
- **EXPERIMENTAL MODEL AND SUBJECT DETAILS**
- **METHOD DETAILS**
 - Plasmid and strain construction
 - Flow cytometry experiments
 - Microfluidics and fluorescent microscopy
 - Mathematical models
 - Simulation of droplet growth and damage repair with the Gillespie algorithm
- **QUANTIFICATION AND STATISTICAL ANALYSIS**
 - Image processing
 - Analysis of single-cell NF- κ B dynamics
 - Statistical analysis

SUPPLEMENTAL INFORMATION

Supplemental information can be found online at <https://doi.org/10.1016/j.cels.2023.04.001>.

ACKNOWLEDGMENTS

This work was supported partly by the National Key R&D Program of China (grant no. 2021YFF1200500, 2019YFA09004500, 2018YFA0902800), National Science Foundation of China (grant no. 31622022, 31470819), and the Strategic Priority Research Program of the Chinese Academy of Sciences (grant no. XDB0480000). Furthermore, this work was supported by the Independent Research Fund Denmark (grant no. 9040-00116B), the Novo Nordisk Foundation (grant no. NNF20OC0064978), the Danish National Research Foundation through StemPhys Center of Excellence (grant no. DNRF116), the Carlsberg Foundation (grant no. CF20-0621), and the Lundbeck Foundation (grant no. R347-2020-2250).

AUTHOR CONTRIBUTIONS

P.W. and M.H.J. conceived the original idea and supervised the project. M.S.H., M.H.J., Y.J., and M.S.N. constructed and interpreted the mathematical model. Y.J., Y.F., W.L., and P.W. designed and performed the experiments. Y.J., Y.F., M.S.H., Z.Z., W.L., L.Q., and P.W. performed data analysis. M.S.H., Y.J., M.H.J., and P.W. wrote the manuscript. Y.F., L.Q., and Q.O. commented and revised the paper.

DECLARATION OF INTERESTS

All authors declare no competing interests.

INCLUSION AND DIVERSITY

We support inclusive, diverse, and equitable conduct of research.

Received: July 4, 2022
Revised: December 16, 2022
Accepted: April 4, 2023
Published: May 17, 2023

REFERENCES

1. Bargiello, T.A., Jackson, F.R., and Young, M.W. (1984). Restoration of circadian behavioural rhythms by gene transfer in *Drosophila*. *Nature* **312**, 752–754.
2. Hardin, P.E., Hall, J.C., and Rosbash, M. (1990). Feedback of the *Drosophila* period gene product on circadian cycling of its messenger RNA levels. *Nature* **343**, 536–540.
3. Thommen, Q., Pfeuty, B., Morant, P.-E., Corellou, F., Bouget, F.-Y., and Lefranc, M. (2010). Robustness of Circadian Clocks to Daylight Fluctuations: Hints from the Picoeucaryote *Ostreococcus tauri*. *PLoS Comput. Biol.* **6**, e1000990.
4. Zehring, W.A., Wheeler, D.A., Reddy, P., Konopka, R.J., Kyriacou, C.P., Rosbash, M., and Hall, J.C. (1984). P-element transformation with period locus DNA restores rhythmicity to mutant, arrhythmic *drosophila melanogaster*. *Cell* **39**, 369–376.
5. Dequéant, M.L., and Pourquié, O. (2008). Segmental patterning of the vertebrate embryonic axis. *Nat. Rev. Genet.* **9**, 370–382.
6. Lauschke, V.M., Tsairis, C.D., François, P., and Aulehla, A. (2013). Scaling of embryonic patterning based on phase-gradient encoding. *Nature* **493**, 101–105.
7. Gupta, A., Wang, Y., and Markram, H. (2000). Organizing principles for a diversity of GABAergic interneurons and synapses in the neocortex. *Science* **287**, 273–278.
8. Power, A.J., Mead, N., Barnes, L., and Goswami, U. (2012). Neural Entrainment to Rhythmically Presented Auditory, Visual, and Audio-Visual Speech in Children. *Front. Psychol.* **3**, 216.
9. Elowitz, M.B., and Leibler, S. (2000). A synthetic oscillatory network of transcriptional regulators. *Nature* **403**, 335–338.
10. Hoffmann, A., Levchenko, A., Scott, M.L., and Baltimore, D. (2002). The IκB-NF- κ B Signaling Module: Temporal Control and Selective Gene Activation. *Science* **298**, 1241–1245.
11. Krishna, S., Jensen, M.H., and Sneppen, K. (2006). Minimal model of spiky oscillations in NF- κ B signaling. *Proc. Natl. Acad. Sci. USA* **103**, 10840–10845.
12. Lahav, G., Rosenfeld, N., Sigal, A., Geva-Zatorsky, N., Levine, A.J., Elowitz, M.B., and Alon, U. (2004). Dynamics of the p53-Mdm2 feedback loop in individual cells. *Nat. Genet.* **36**, 147–150.
13. Nelson, D.E., Ihekweazu, A.E.C., Elliott, M., Johnson, J.R., Gibney, C.A., Foreman, B.E., Nelson, G., Sée, V., Horton, C.A., Spiller, D.G., et al. (2004). Oscillations in NF- κ B Signaling Control the Dynamics of Gene Expression. *Science* **306**, 704–708.
14. Stricker, J., Cookson, S., Bennett, M.R., Mather, W.H., Tsimring, L.S., and Hasty, J. (2008). A fast, robust, and tunable synthetic gene oscillator. *Nature* **456**, 516–519.
15. Helberg, M.L., Krishna, S., Kadanoff, L.P., and Jensen, M.H. (2021). A tale of two rhythms: Locked clocks and chaos in biology. *Cell Syst.* **12**, 291–303.
16. Purvis, J.E., and Lahav, G. (2013). Encoding and Decoding Cellular Information through Signaling Dynamics. *Cell* **152**, 945–956.
17. Helberg, M.S., Lucchetti, A., Hsieh, F.-S., Minh Nguyen, D.P., Chen, S.-h., and Jensen, M.H. (2022). Enhanced DNA repair through droplet formation and p53 oscillations. *Cell* **185**, 4394–4408.e10.
18. Arnol'd, V.I. (1965). Small denominators. I. Mappings of the circumference onto itself. *American Mathematical Society Translations: Series 2* **46**, 213–284.
19. Jensen, M.H., Bak, P., and Bohr, T. (1984). Transition to chaos by interaction of resonances in dissipative systems. I: Circle maps. *Phys. Rev. A* **30**, 1960–1969.

20. Heltberg, M.L., Krishna, S., and Jensen, M.H. (2019). On chaotic dynamics in transcription factors and the associated effects in differential gene regulation. *Nat. Commun.* **10**, 71–10.
21. García-Ojalvo, J., Elowitz, M.B., and Strogatz, S.H. (2004). Modeling a synthetic multicellular clock: repressilators coupled by quorum sensing. *Proc. Natl. Acad. Sci. USA* **101**, 10955–10960.
22. Grabe, S., Mahammadov, E., Olmo, M.d., and Herzel, H. (2021). Synergies of Multiple Zeitgebers Tune Entrainment. *Front. Netw. Physiol.* **1**, 803011.
23. Koronowski, K.B., and Sassone-Corsi, P. (2021). Communicating clocks shape circadian homeostasis. *Science* **371**, eabd0951.
24. Mondragón-Palomino, O., Danino, T., Selimkhanov, J., Tsimring, L., and Hasty, J. (2011). Entrainment of a Population of Synthetic Genetic Oscillators. *Science* **333**, 1315–1319.
25. Relógio, A., Westerman, P.O., Wallach, T., Schellenberg, K., Kramer, A., and Herzel, H. (2011). Tuning the Mammalian Circadian Clock: Robust Synergy of Two Loops. *PLoS Comput. Biol.* **7**, e1002309.
26. Sonnen, K.F., Lauschke, V.M., Uraji, J., Falk, H.J., Petersen, Y., Funk, M.C., Beaupeux, M., François, P., Merten, C.A., and Aulehla, A. (2018). Modulation of Phase Shift between Wnt and Notch Signaling Oscillations Controls Mesoderm Segmentation. *Cell* **172**, 1079–1090.e12.
27. Zhang, Z.-B., Wang, Q.-y., Ke, Y.-X., Liu, S.-Y., Ju, J.-Q., Lim, W.A., Tang, C., and Wei, P. (2017). Design of Tunable Oscillatory Dynamics in a Synthetic NF-κB Signaling Circuit. *Cell Syst.* **5**, 460–470.e5.
28. Gillespie, D.T. (1977). Exact Stochastic Simulation of Coupled Chemical Reactions. *J. Phys. Chem.* **81**, 2340–2361.
29. Wolf, A., Swift, J.B., Swinney, H.L., and Vastano, J.A. (1985). Determining Lyapunov exponents from a time series. *Phys. Nonlinear Phenom.* **16**, 285–317.
30. van der Pol, B. (1926). On "relaxation oscillations. *Lond. Edinb. Dublin Philos. Mag. J. Sci.* **2**, 978–992.
31. Mengel, B., Hunziker, A., Pedersen, L., Trusina, A., Jensen, M.H., and Krishna, S. (2010). Modeling oscillatory control in NF-κB, p53 and Wnt signaling. *Curr. Opin. Genet. Dev.* **20**, 656–664.
32. Cai, L., Dalal, C.K., and Elowitz, M.B. (2008). Frequency-modulated nuclear localization bursts coordinate gene regulation. *Nature* **455**, 485–490.
33. Hao, N., and O'Shea, E.K. (2011). Signal-dependent dynamics of transcription factor translocation controls gene expression. *Nat. Struct. Mol. Biol.* **19**, 31–39.
34. Heltberg, M., Kellogg, R.A., Krishna, S., Tay, S., and Jensen, M.H. (2016). Noise Induces Hopping between NF-κB Entrainment Modes. *Cell Systems* **3**, 532–539.e3.
35. Ashall, L., Horton, C.A., Nelson, D.E., Paszek, P., Harper, C.V., Sillitoe, K., Ryan, S., Spiller, D.G., Unitt, J.F., Broomhead, D.S., et al. (2009). Pulsatile Stimulation Determines Timing and Specificity of NF-κB-Dependent Transcription. *Science* **324**, 242–246.
36. Kim, J.K., and Tyson, J.J. (2020). Misuse of the Michaelis–Menten rate law for protein interaction networks and its remedy. *PLoS Comput. Biol.* **16**, e1008258.
37. Kuramoto, Y. (1984). *Chemical Oscillations, Waves, and Turbulence* (Berlin, Heidelberg: Springer).
38. Komarov, M., and Pikovsky, A. (2013). Multiplicity of singular synchronous states in the Kuramoto model of coupled oscillators. *Phys. Rev. Lett.* **111**, 204101.
39. Matthews, P.C., Mirollo, R.E., and Strogatz, S.H. (1991). Dynamics of a large system of coupled nonlinear oscillators. *Phys. Nonlinear Phenom.* **52**, 293–331.
40. Strogatz, S.H. (2000). From Kuramoto to Crawford: exploring the onset of synchronization in populations of coupled oscillators. *Phys. Nonlinear Phenom.* **143**, 1–20.
41. Bordugov, G., Abraham, U., Granada, A., Rose, P., Imkeller, K., Kramer, A., and Herzel, H. (2015). Tuning the phase of circadian entrainment. *J. R. Soc. Interface* **12**, 20150282.
42. Pfeuty, B., Thommen, Q., Corellou, F., Djouani-Tahri, E.B., Bouget, F.-Y., and Lefranc, M. (2012). Circadian clocks in changing weather and seasons: Lessons from the picoalga *Ostreococcus tauri*. *Bioessays* **34**, 781–790.
43. Pfeuty, B., Thommen, Q., and Lefranc, M. (2011). Robust entrainment of circadian oscillators requires specific phase response curves. *Biophys. J.* **100**, 2557–2565.
44. Kim, J.K., Forger, D.B., Marconi, M., Wood, D., Doran, A., Wager, T., Chang, C., and Walton, K.M. (2013). Modeling and Validating Chronic Pharmacological Manipulation of Circadian Rhythms. *CPT Pharmacometrics Syst. Pharmacol.* **2**, e57–e11.
45. Kim, D.W., Chang, C., Chen, X., Doran, A.C., Gaudreault, F., Wager, T., DeMarco, G.J., and Kim, J.K. (2019). Systems approach reveals photosensitivity and PER2 level as determinants of clock-modulator efficacy. *Mol. Syst. Biol.* **15**, e8838.
46. Meng, Q.-J., Maywood, E.S., Bechtold, D.A., Lu, W.Q., Li, J., Gibbs, J.E., Dupré, S.M., Chesham, J.E., Rajamohan, F., Knafoels, J., et al. (2010). Entrainment of disrupted circadian behavior through inhibition of casein kinase 1 (CK1) enzymes. *Proc. Natl. Acad. Sci. USA* **107**, 15240–15245.
47. Gupta, A., Hepp, B., and Khammash, M. (2016). Noise Induces the Population-Level Entrainment of Incoherent, Uncoupled Intracellular Oscillators. *Cell Syst.* **3**, 521–531.e13.
48. Kim, J.K., Josić, K., and Bennett, M.R. (2015). The relationship between stochastic and deterministic quasi-steady state approximations. *BMC Syst. Biol.* **9**, 87.
49. Song, Y.M., Hong, H., and Kim, J.K. (2021). Universally valid reduction of multiscale stochastic biochemical systems using simple non-elementary propensities. *PLoS Comput. Biol.* **17**, e1008952.

STAR★METHODS

KEY RESOURCES TABLE

REAGENT or RESOURCE	SOURCE	IDENTIFIER
Bacterial and virus strains		
DH5 α Competent Cell	Transgene	CD201
Biological samples		
Tris	Amresco	0826
EDTA	Amresco	N470
Salmon Sperm DNA	Invitrogen	15632011
Poly (ethylene glycol)	Sigma-Aldrich	P4338
α -factor	GenScript	RP01002
Doxycycline hyclate	Sigma-Aldrich	D9891
Concanavalin A	Sigma-Aldrich	C2010
Pronase	Roche	11459643001
AarI restriction enzyme	Thermo Fisher Scientific	ER1581
Q5 High-Fidelity 2 \times Master Mix	NEB	M0492L
T4 DNA Ligase	NEB	M0202L
2 \times Taq PCR MasterMix	TIANGEN	KT201
Lethal Based Fast Cloning Kit	TIANGEN	VT205
TIANprep Midi Plasmid Kit	TIANGEN	DP106
Universal DNA Purification Kit	TIANGEN	DP214
Lithium acetate	Sigma-Aldrich	517992
Deposited data		
Raw and analyzed data	Zenodo	https://doi.org/10.5281/zenodo.7694120
Experimental models: Organisms/strains		
scLW009: Yeast strain for double input sensing. Genotype: CB008; pADH1-rtTA; pTet07-3xFlag-RelA-GFP; pUra3-NES-Cdc4; pNFkBcyc1_2(PspOMI Mig1)-1 \times flag-IkB α -ppDeg	This study	N/A
scLW013: Yeast strain for FACS analysis of the dual response promoter. Genotype: CB008; pADH1-rtTA; pTet07-3xFlag-RelA-GFP; pUra3-NES-Cdc4; pNFkBcyc1_2(PspOMI Mig1)_mCherry; pUra3-1 \times Flag-IkB α -ppDeg	This study	N/A
scJYX001: Yeast strain for downstream protein production assay. Genotype: CB008; pADH1-rtTA; pTet07-3xFlag-RelA-GFP; pUra3-NES-Cdc4; pNFkBcyc1_2(PspOMI Mig1)-1 \times flag-IkB α -ppDeg; pNFkB070-1 \times Flag-mCherry	This study	N/A
Recombinant DNA		
pZBZ070 pNFkB070-1 \times Flag-mCherry	Zhang et al. ²⁷	N/A
pZBZ219 pNFkBcyc1_2(PspOMI Mig1)-1 \times flag-IkB α -ppDeg	Zhang et al. ²⁷	N/A
pLW012 pNFkBcyc1_2(PspOMI Mig1)_mCherry	This study	N/A
Software and algorithms		
NIS-Elements	Nikon	N/A

(Continued on next page)

Continued

REAGENT or RESOURCE	SOURCE	IDENTIFIER
ImageJ	NIH	https://imagej.nih.gov/ij/
FlowJo	FlowJo	https://www.flowjo.com/
CellASIC ONIX2 FG	Millipore Sigma	N/A
MATLAB R2020a	MathWorks	https://www.mathworks.com/
Original Codes	Zenodo	10.5281/zenodo.7694120
Other		
CellASIC Y04D microfluidic plates	EMD Millipore	Y04C-02-5PK
CellASIC ONIX microfluidic platform	EMD Millipore	EV262

RESOURCE AVAILABILITY

Lead contact

Further information and requests for resources and reagents should be directed to and will be fulfilled by the lead contact, Ping Wei (ping.wei@siat.ac.cn).

Materials availability

This study did not generate new unique reagents.

Data and code availability

Data have been deposited at Zenodo and are publicly available as of the date of publication. DOIs are listed in the [key resources table](#).

Original code has been deposited at Zenodo and are publicly available as of the date of publication. DOIs are listed in the [key resources table](#).

Any additional information required to reanalyze the data reported in this paper is available from the lead contact upon request.

EXPERIMENTAL MODEL AND SUBJECT DETAILS

All yeast strains used in this study and the figures where each strain is used are listed in [key resources table](#). Unless otherwise specified, the parent yeast strain for all our synthetic strains was CB008 (W303 MAT α Δfar1 Δhis3 Δtrp1 Δleu2 Δura3). The deletion of FAR1 gene allowed the cells to response to α -factor stimulation without arresting their cell cycle. The growth conditions are described as below.

METHOD DETAILS

Plasmid and strain construction

The protocols for plasmids and strain construction were based on the work of Zhang et al.²⁷ Briefly, all plasmids used in this study were constructed by using standard protocols and were replicated in DH5 α , *Escherichia coli*. All constructs were confirmed by colony PCR and sequencing. The double-input responding promoter was constructed by fusing 2 repeats of a stress response element and 4 repeats of the κB binding site in series, upstream to an engineered yeast CYC1 promoter. Yeast transformations were done with the standard LiAc method. The engineered genetic components were integrated in a single copy into the genome through a set of integrating yeast vectors (pNH603, pNH604, pNH605, pNH606, pNH607). All yeast genomic integrations were confirmed by yeast colony PCR.

Flow cytometry experiments

Analysis of the induced expression level of the hybrid promoter was performed by measuring fluorescent protein (mCherry) intensity with a Becton Dickinson LSRII flow cytometer (high throughput sampler equipped). For all FACS experiments, single colony was picked from YPD agar plates and triplicate cultures were grown in transparent synthetic complete dropout media at 30°C overnight in a shaking incubator. The overnight cultures were diluted to an OD₆₀₀ of 0.05 and grown to log phase (OD₆₀₀ = 0.3–0.6). 100 μ L aliquots was taken for flow cytometer measurements and 10,000 cells were counted for each reading. To survey the expression of mCherry as a result of different input types, 10 μ M α -factor alone, 2.5% ethanol alone or α -factor combined with ethanol were added into the wells and the fluorescence levels were measured after 2h. 5 μ g/mL doxycycline (Sigma-Aldrich) was added into each separate sample throughout the culture for induction of NF-κB-GFP proteins.

Microfluidics and fluorescent microscopy

The microfluidic cell cultures were performed in Y04C yeast perfusion plates with an ONIX flow control system (Millipore). Single colony was picked from YPD agar plates and cultures were grown in transparent synthetic complete dropout media at 30°C overnight in a shaking incubator. The overnight cultures were diluted to an OD₆₀₀ of 0.05 and grown to log phase (OD₆₀₀ = 0.3–0.6). Before loading cells, the flow chamber was pre-coated with synthetic complete dropout media. Once loaded, cells were flowed over by synthetic complete dropout media for 30 min before applying 10 μM α-factor (GenScript) stimulation which was dissolved in the media. The periodic stimulation experiments of time variant inputs were achieved by precise control of media flow into the imaging chamber. The stimulations were all in square-wave forms. Therefore, all conditions of combined periodic α-factor and ethanol can be considered as a repeat of 4 basic stages (α-factor present, ethanol present, both present, both absent) with different time depending on the phase and period values. All programs were designed to expose activated wells within the microfluidic plate to 2 psi. Image acquisition was performed with a TE2000-E automated inverted microscope (Nikon) with perfect focus system and the Andor Neo 5.5 sCMOS camera (ANDOR Technology Ltd). Images were acquired with a 100× Plan Apo oil immersion lens (NA 1.40) with a time interval of 3 min to trace NF-κB dynamics, and a time interval of 10 min to trace the downstream protein expression. Cells in the microfluidic plate were maintained at 30°C.

Mathematical models

As for the modeling of RelA dynamics, our mathematical approach was inspired by the model published by Zhang et al.²⁷ This model includes 12 variables and our aim was to construct a mathematical model that did capture the core dynamics of RelA. We therefore focused on the deactivation of RelA due to the interactions with IκB and based on this we formed a negative feedback loop with only 4 variables, assuming a constant total level of RelA. Mathematically these are described as:

$$\frac{dR_C}{dt} = k_d C - k_a R_C I + k_{eN} k_v R_N - k_{IN} R_C + V_m \frac{C}{C + K_m} \quad (1)$$

$$\frac{dC}{dt} = k_a R_C I - k_d C - V_m \frac{C}{C + K_m} \quad (2)$$

$$\frac{dI}{dt} = k_d C - k_a R_C I - V_m \frac{I}{I + K_m} + k_{trt} m_I \quad (3)$$

$$\frac{dm_I}{dt} = k_v \left(V_h \frac{(k_v R_N)^h}{k_h^h + (k_v R_N)^h} - k_{etm} m_I \right) \quad (4)$$

$$R_N = R_{tot} - R_c - C \quad (5)$$

Here R_C , C , I and m_I denote for the concentration of cytoplasmic RelA, RelA-IκB complex, free IκB protein and mRNA of IκB, respectively. Meanings of the parameters can be found in Table S1. In this we incorporate the effect of the α-factor in the constant K_m so this takes the form: $K_m \rightarrow K_m \frac{1}{1 + \delta_1 \alpha}$ effect of $V_h \rightarrow V_h \frac{1}{1 + \delta_2 E}$. These equations can schematically be visualized as the genetic network shown in Fig. S2A. Based on the parameters used in the work of Zhang et al., we tested that this model did not show oscillations in the absence of α-factor, but upon stimulation of this started to oscillate as is found in the experimental observations. This we did recapture, where we find that the oscillations quickly settle into the stable limit cycle, seen both in the time trace (Fig. S2B, above) and in the phase space spanned by RelA and IκB (Fig. S2B, below). Then we tested if this model resulted in oscillations with a period of approximately 24 min, and this was found by performing the FFT analysis, where the largest power was found for a period of 24.1 min (Fig. S2C). Finally, we simulated the model with stochastic noise levels, by implementing the Gillespie algorithm. This we did first for an oscillatory level of α-factor (Fig. S2D, left) and later for a constant level of α-factor and oscillatory level of ethanol (Fig. S2D, right). These results captured the observed dynamics of RelA in this system, and therefore we conclude that we had successfully derived a new model for the dynamics of RelA, that is greatly simplified compared to the previous model published by Zhang et al.

In order to model the downstream effects of the dynamics in RelA, we incorporated a previously published by Heitberg et al.³⁴

$$\frac{dm}{dt} = k_1 \frac{R_N^n}{R_N^n + k_2^n} - k_3 m \quad (6)$$

$$\frac{dP}{dt} = k_4 m - k_5 P \quad (7)$$

In this model, m is the mRNA for a particular protein, denoted by P . The production is stimulated by the concentration in the nucleus of RelA through a hill term. From this, the protein production is linearly dependent on the amount of mRNA. With this model, we can describe different types of genes, depending on their affinity (k_2) and cooperativity (n) to RelA.

Simulation of droplet growth and damage repair with the Gillespie algorithm

In the Gillespie algorithm we consider a volume V , with a spatially uniform mixture of N chemical species that can react through M different reactions, $R_1 \dots R_M$. The number of each of the species is denoted $X_1 \dots X_N$. At $t = 0$, we thus consider the initial number of molecules and calculates all reactions. The first goal is now to calculate the PDF, for the time until the next reaction occurs.

We consider the probability that the next reaction is of type ε , and it occurs in the time interval $[t + \tau, t + \tau + dt]$. We therefore consider:

$$P(\tau, \varepsilon)dt = P_{not}(\tau) \cdot R_\varepsilon dt$$

Therefore, we want to describe $P_{not}(\tau)$ in terms of the rates. Since at each timestep ε , the probability for no reaction to appear is:

$$P_{not}(dt) = 1 - \sum_{i=1}^M R_i dt$$

We can thus define $\tau \equiv n \cdot dt$ and then:

$$P_{not}(\tau) = P_{not}(dt)^n = \left(1 - \sum_{i=1}^M R_i dt\right)^n \approx e^{-R_{tot}\tau}$$

We can thus calculate the time until the next event as

$$T_{event} = \frac{-\ln(\mathcal{R})}{\sum \mu_i}$$

where \mathcal{R} is a random number, uniformly distributed between 0 and 1. Then, in order to find which of the possible events take place, we assign a number to each reaction rate and choose the reaction, m , that satisfies:

$$\frac{\sum_{i=1}^{m-1} \mu_i}{\sum_{i=1}^N \mu_i} \leq \mathcal{R} < \frac{\sum_{i=1}^m \mu_i}{\sum_{i=1}^N \mu_i}$$

After each event we update all the rates, and then repeat the steps.

In the system of ordinary differential equations, we therefore coarse-grain the system and turn each term into a rate that can either add or remove a single molecule from the total number of molecules. With this algorithm one can therefore simulate the system, based on single proteins dynamics, in the presence of intrinsic noise. We note that since our equations have been derived in the quasi-steady state approximation, the direct application of the Gillespie algorithm can lead to inaccurate estimation of the noise level, in general to an underestimation of stochasticity compared to the full system.^{48,49} However, this potential imprecision does not affect the main results, since the stochasticity is mainly responsible for generating a standard deviation in the periodicity and we are interested in studying the relative effect of the addition of two external oscillatory signals. If we claimed that the noise we generate in the system correspond directly to the fluctuations observed in the experiments, these imprecisions could have caused significant limitations to the results, but since we study a relative effect, using the same algorithm, we argue that these effects will not significantly alter the results of this work. Finally, we also note that the results for stochastic noise in the Van der Pol oscillator in Figure 4, is generated using Langevin simulations, which is exact for this system. The fact that we obtain similar results is also reassuring that the approximations using Gillespie algorithm for an approximated system, does not change the main conclusion of the stochastic results.

QUANTIFICATION AND STATISTICAL ANALYSIS

Image processing

We monitored the NF-κB dynamic behaviors of our synthetic signaling circuit by live single-cell fluorescent microscopy. Based on bright field images, cell segmentation and tracing were done automatically by customized MATLAB software cellseg. The backgrounds of all fluorescence images were first subtracted by ImageJ (1.49v, Java1.6.024, 64 bit). The single-cell dynamics data were then extracted from these processed time-lapsed fluorescence images also by cellseg. Within the boundary of one yeast cell, we quantified the average intensity of the brightest 10×10 NF-κB pixels as nuclear NF-κB concentration, and the average intensity of all pixels as total NF-κB concentration. We used the nuclear to total ratio of NF-κB concentration as nuclear NF-κB index which was denoted as Nuc.NF-κB. The time series of single-cell Nuc.NF-κB was acquired automatically by customized MATLAB programs. Each single-cell trajectory was smoothed by a Savitzky-Golay filter of degree 2 before further analysis.

Analysis of single-cell NF-κB dynamics

For the single-cell nuclear import dynamics data, we did a two-step analysis to extract parameters to describe the response. First, we took moving average of the data with a step length of 5 to smooth out impulse response. Oscillatory properties including period T, peak amplitude A, peak phase ψ were quantified by a custom-made MATLAB program for peak detection in single-cell Nuc.NF-κB trajectories. Briefly, all the local maximum and local minimum in the trajectories were first picked out. We then calculate the difference between every adjacent maximum-minimum pairs (A), as well as the time interval between two adjacent minima (T). Thus, each peak can be characterized by the aforementioned parameters, and corresponds to a certain point in the 2D parameter space. Since the primary data contains considerable level of noises, which were caused by both technical and biological reasons, we first took the no-input condition (only doxycycline present) as a negative control, and plotted the peaks on the parameter space with their A and T values. A boundary was drawn to gate these points, and for the rest of experiments, all peaks inside this gate were considered as experimental noise and omitted. Only the remaining peaks were considered as valid and used for further analysis. The peak phase is defined by the time difference between the peaking time point and the most recent time point when media with α -factor began to flow into the chamber, this value was further divided by the input period and mapped to the range of 0– 2π . The EI was defined as follows:

$$EI = 1 - \frac{-\sum_{i=1}^n P_i \ln P_i}{\ln N}$$

We calculated this index by first divide all the peak phases into 9 bins (N), and P_i denotes for the frequency of phases in each bin. A uniform distribution would result in $EI = 0$, while $EI = 1$ can only be achieved when all phases are equal.

To calculate the oscillatory period of the RelA dynamics we applied two methods: FFT and a standard peak finding algorithm. For the FFT, we applied the algorithm adopted into MATLAB, and found the largest value as a representation of the oscillation frequency. To remove underlying effects, we denoised the data, by subtracting a third order polynomial, fitted to the raw data.

Statistical analysis

Statistical parameters were reported in the figures and figure legends. All statistical analysis was performed in MATLAB R2020a (MathWorks).